



Propagation of partially coherent fields radiated by sources with univariable cross-spectral density

Massimo Santarsiero¹, Rosario Martínez-Herrero², Juan Carlos González de Sande³ , Gemma Piquero^{2,*} , Olga Korotkova⁴, and Franco Gori¹

¹ DIEM, Università Roma Tre, via V. Volterra 62, Rome 00146, Italy

² Departamento de Óptica, Fac. CC. Físicas, U.C.M., Ciudad Universitaria s/n, 28040 Madrid, Spain

³ Universidad Politécnica de Madrid, ETSIS de Telecomunicación, Campus Sur, 28031 Madrid, Spain

⁴ Department of Physics, University of Miami, 1320 Campo Sano Drive, Coral Gables, FL, 33146, USA

Received 18 December 2025 / Accepted 4 February 2026

Abstract. A new class of partially coherent light sources, the sources with uni-variable cross-spectral density (CSD), has been recently introduced. Their CSD is obtained starting from any function of a single complex argument having non-negative Taylor coefficients. This allows the conception of a virtually infinite number of physically realizable partially coherent sources. Here, the main characteristics of sources of this class are investigated through examples, with particular reference to the irradiance and coherence properties across the source plane and upon propagation, both in the near and in the far field. Furthermore, since the coherent modes of such sources present optical vortices, parameters quantifying the vortex structure of the field across the source plane are also evaluated for the presented cases.

Keywords: Coherence, Coherent modes, Propagation, Optical vortices, Orbital angular moment, Structured coherence.

1 Introduction

Structured light has attracted strong interest in recent years, largely driven by its wide range of applications and by rapid progress in generating and detecting tailored optical fields [1, 2]. Within this area, partially coherent sources are increasingly regarded not as a limitation but as a useful degree of freedom, since the engineering of spatial coherence can mitigate drawbacks of highly coherent beams. Recent reviews emphasize that partially coherent beams with structured coherence have been explored for concrete applications including: optical imaging [3, 4], free-space optical communications with improved robustness to atmospheric turbulence [5–8], coherence-based optical encryption and robust signal/information transmission through complex or scattering media [8, 9], optical manipulation [10, 11], and remote sensing [12]. These are some of the reasons why there is great interest in devising, realizing, and characterizing new light sources, both coherent and partially coherent, that allow the characteristics of the light radiated by these sources to be modified in a controlled way [13–38].

Interesting and promising results are derived from the presence of phase vortices, which confer unique capabilities

to the beam radiated from the source [5, 6, 12, 39–54]. For example, they find application in optical manipulation, because they can exert torque on microscopic particles, enabling advanced optical tweezers and micromanipulation [10, 46]; in imaging and metrology, where they offer new possibilities for super-resolution or phase-sensitive detection [12, 44]; in optical communication, since they provide an extra degree of freedom, the orbital angular momentum (OAM), for multiplexing and increasing data capacity [5, 6]. Vortex beams are typically generated using elements such as spiral phase plates, computer-generated holograms, q plates, or metasurfaces that encode the desired OAM mode [47, 50, 51, 53].

Recently, a new type of partially coherent light source, namely, a source with uni-variable cross-spectral density (CSD), has been proposed [38]. The peculiarity of sources of this class is that their CSD [55] can be directly derived from a function of a single complex variable [38]. The only requirement this function has to fulfill in order for it to be associated with a well-defined CSD is that its Taylor expansion must involve only non-negative coefficients. Several analytical forms, in some cases very simple, of bona-fide CSD can be devised in this way. Sources with uni-variable CSD are defined within a finite circular region, related to the convergence domain of the above Taylor series, and

* Corresponding author: piquero@ucm.es

can be expressed as the superposition of coherent modes [55] carrying optical vortices. The analytical form of the vortex modes is quite simple, both across the source plane and in the far zone, enabling the study of the coherence features of the source, as well as those of the field radiated under Fraunhofer conditions [38]. One of the important features of univariable CSDs is their capability to customize at will the contributions from various coherent modes, serving, at the same rate, as the OAM modes. This renders them ideal for high-capacity information-transfer applications employing structured light.

The main aim of the present paper is, on one hand, to extend to the Fresnel regime the study of the propagation of beams radiated from sources with uni-variable CSD; on the other hand, to study the effects of truncating the number of the modes involved in the expansion. Examples will be presented concerning the so-called sZegő source, introduced in [38], which is obtained with an infinite number of Taylor terms, all with the same coefficient. Taking only a finite number of terms gives rise to the truncated sZegő source, introduced here, which represents a more realistic model for a partially coherent source, suitable to be physically realized. Finally, hints for devising other types of uni-variable CSDs are given for some cases in which the CSD takes a simple closed form.

2 Preliminaries

2.1 Uni-variable CSDs

A uni-variable CSD [38] is defined from any function g of a single complex variable ζ such that:

$$g(\zeta) = \sum_{n=0}^{\infty} c_n \zeta^n, \quad (1)$$

where

$$c_n \geq 0 \quad (\forall n), \quad (2)$$

and ζ belongs to the convergence domain of the series. By suitably scaling the argument of g it is always possible to set such a domain as

$$|\zeta| < 1. \quad (3)$$

The CSD associated with g is obtained by letting

$$\zeta = \frac{r_1 r_2}{r_0^2} e^{i(\varphi_1 - \varphi_2)}, \quad (4)$$

where (r_1, φ_1) and (r_2, φ_2) are the polar coordinates of two points across the source plane (\mathbf{r}_1 and \mathbf{r}_2) and r_0 is the radius of the circular region where the source is defined. It should be noted that although the CSD depends on two points, for this class of sources, the dependence enters only through the single complex parameter ζ , following the terminology introduced previously in reference [38]. Therefore, using equations (1) and (4) we define, across the plane $z = 0$,

$$\begin{aligned} W(\mathbf{r}_1, \mathbf{r}_2, 0) &= g\left(\frac{r_1 r_2}{r_0^2} e^{i(\varphi_1 - \varphi_2)}\right) \\ &= \sum_{n=0}^{\infty} c_n \left(\frac{r_1 r_2}{r_0^2}\right)^n e^{in(\varphi_1 - \varphi_2)}, \quad (5) \\ &(|r| < r_0). \end{aligned}$$

The sum in equation (5) can be read as the Mercer expansion of W_0 , that is, [55]

$$W(\mathbf{r}_1, \mathbf{r}_2, 0) = \sum_{n=0}^{\infty} \lambda_n \Phi_n(\mathbf{r}_1, 0) \Phi_n^*(\mathbf{r}_2, 0), \quad (6)$$

with coherent modes (taking into account their normalization) given by

$$\begin{aligned} \Phi_n(\mathbf{r}, 0) &= \sqrt{\frac{n+1}{\pi r_0^2}} \left(\frac{r}{r_0}\right)^n \text{circ}\left(\frac{r}{r_0}\right) e^{in\varphi}, \quad (7) \\ &(n = 0, 1, \dots), \end{aligned}$$

and eigenvalues

$$\lambda_n = c_n \frac{\pi r_0^2}{n+1}, \quad (n = 0, 1, \dots), \quad (8)$$

where $\text{circ}(r)$ is the characteristic function of a unit disk centered at the origin of the axes. The second argument of the modes Φ_n refers to the z -coordinate of the transverse plane where they are evaluated (in this case, across the source, that is, $z = 0$). The condition in equation (2), together with equation (8), guarantees that $\lambda_n > 0$ ($\forall n$), so that the CSD turns out to be well defined [13, 14].

The modes in equation (7) are recognized at once as optical vortices [49] with charge n . They have the same structure as Laguerre–Gaussian beams [56] in which the Laguerre polynomial has order zero and where the Gaussian function has been replaced by a circ .

The number of genuine CSDs that can be obtained following the present approach is practically unlimited, the only constraint that the function g has to fulfill being the fact that the coefficients of its Taylor expansion are all non-negative. Examples will be given in the following, where simple forms of CSDs will be presented, together with the mean features of the beams they radiate.

2.2 Characterization of uni-variable CSDs in OAM space

Uni-variable CSD represents one of a few known model optical fields that carry OAM in multiple modes, either finite or infinite. For the characterization of radial-only correlations among the OAM modes in such fields, the coherence-orbital angular momentum (COAM) matrix $\overline{W}(\rho_1, \rho_2, z)$ and its derivatives can be used [57]. Each element of the COAM matrix is a scalar radial field correlation at a pair of OAM indices, given by the expression:

$$\begin{aligned}
 W_{\ell m}(r_1, r_2, z) &= \frac{1}{4\pi^2} \int_0^{2\pi} \int_0^{2\pi} W(r_1, r_2, z) e^{-i(\ell\varphi_1 - m\varphi_2)} d\varphi_1 d\varphi_2, \\
 &-\infty < \ell, m < \infty.
 \end{aligned} \tag{9}$$

The COAM matrix is the counterpart of the CSD matrix defined in polarization space to the OAM space and carries similar properties (quasi-Hermiticity, non-negative definiteness, etc.). However, it can have any size, say $L \times L$, where L is the largest by magnitude OAM index involved. Also, for theoretical models, infinitely dimensional matrices are possible with certain convergence constraints. The uni-variable beam model is of this type.

Two derivatives of the COAM matrix are important and will be considered here. First, the OAM degree of coherence is the analog of the EM degree of coherence in the OAM space [58]:

$$o(r_1, r_2, z) = \frac{\sqrt{\text{Tr}[\overrightarrow{W}^\dagger(r_1, r_2, z) \overrightarrow{W}(r_1, r_2, z)]}}{\prod_{j=1,2} \sqrt{\text{Tr} \overrightarrow{W}(r_j, r_j, z)}}. \tag{10}$$

It provides the cumulative information about the normalized correlations at a pair of radii for all pairs of the OAM modes, regardless of the OAM phase information contained in each mode.

Second, it was found that a harmonic beam carrying OAM in L modes traces an orbitalization ellipse in LD OAM space (polar Fourier space) at a fixed radius [59], analogously to the two/three component electric field tracing a polarization ellipse in real 2D/3D space. To extend this geometric description to partially coherent beams, the COAM matrix can be considered at a single radius $r_1 = r_2 = r$, and regarded as the $L \times L$ orbitalization matrix [60]:

$$\overrightarrow{O}(r, z) = \overrightarrow{W}(r, r, z), \tag{11}$$

the term stemming from its formal similarity to a polarization matrix. In LD the orbitalization matrix is shown to decompose into three parts: completely orbitalized, unorbitalized, and partially orbitalized, in which mixing occurs for mode couples, triples, ..., up to $L - 1$. The completely orbitalized matrix is shown to factorize, representing a beam indistinguishable from harmonic, and, hence, described by an orbitalization ellipse. The contribution of the intensity of the completely orbitalized portion of the beam in the total beam, at a fixed radius, was introduced as the degree of orbitalization [60]:

$$O(r, z) = \frac{\sigma_0(r, z) - \sigma_1(r, z)}{\sum_{n=0}^{\infty} \sigma_n(r, z)}, \tag{12}$$

where $\sigma_0(r, z) \geq \sigma_1(r, z) \geq \dots \geq \sigma_L(r, z) \geq \dots$ is the ordered sequence of the eigenvalues of \overrightarrow{O} , all being real and nonnegative due to its Hermiticity and non-negative-definiteness. This quantity is analogous in nature to

the degree of polarization and reduces to it in form for $L = 2$ and 3. In this work, we will thoroughly examine its behavior for uni-variable beams.

We note that for a univariable CSD the COAM matrix is diagonal and hence the calculations of both derivatives are relatively simple. For example, the OAM DOC becomes

$$o(r_1, r_2, 0) = \frac{\sqrt{\sum_{n=0}^{\infty} c_n^2 (r_1 r_2 / r_0^2)^{2n}}}{\prod_{j=1,2} \sqrt{\sum_{n=0}^{\infty} c_n (r_j / r_0)^n}}. \tag{13}$$

As we show below, for uni-variable beams σ_0 and σ_1 may depend on different c_n at different radii and, hence, it appears impossible to write down an explicit single formula for the degree of orbitalization. Instead, a piecewise-continuous function will be used, with its interval endpoints determined numerically.

3 Beams radiated by uni-variable CSDs

The propagation from sources with uni-variable CSD, both in the near and in the far field, can be dealt with starting from their expansion in terms of coherent modes. In such a way, from equation (6) we have, at any plane $z = \text{const.}$,

$$W(\mathbf{r}_1, \mathbf{r}_2, z) = \sum_{n=0}^{\infty} \lambda_n \Phi_n(\mathbf{r}_1, z) \Phi_n^*(\mathbf{r}_2, z), \tag{14}$$

where the expression of the propagated modes $\Phi_n(\mathbf{r}, z)$ depends on the approximation we use.

Using the expression above, the spectral density and the degree of coherence of the radiated field can be evaluated as [55]

$$S(\mathbf{r}, z) \equiv W(\mathbf{r}, \mathbf{r}, z) = \sum_{n=0}^{\infty} \lambda_n |\Phi_n(\mathbf{r}, z)|^2, \tag{15}$$

and

$$\mu(\mathbf{r}_1, \mathbf{r}_2, z) \equiv \frac{W(\mathbf{r}_1, \mathbf{r}_2, z)}{\sqrt{S(\mathbf{r}_1, z) S(\mathbf{r}_2, z)}}, \tag{16}$$

respectively.

3.1 Coherent modes in paraxial regime

Within the paraxial approximation, the propagation of the modes can be studied through the Fresnel integral, which, for a typical field $V(r, \varphi, z)$, in polar coordinates reads [55]

$$\begin{aligned}
 V(r, \varphi, z) &= -\frac{ik e^{ikz}}{2\pi z} \int_0^{\infty} \int_0^{2\pi} \\
 V(r', \varphi', 0) &e^{\frac{ik}{2z} [r'^2 + r^2 - 2r'r \cos(\varphi' - \varphi)]} r' dr' d\varphi'.
 \end{aligned} \tag{17}$$

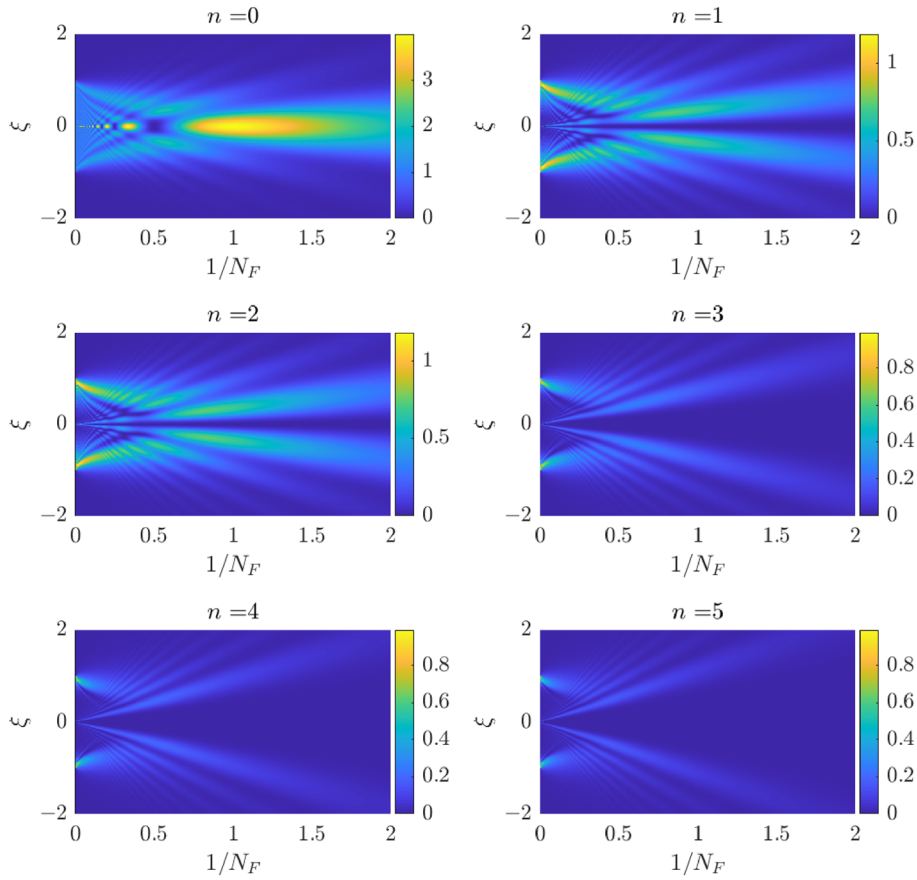


Fig. 1. Density plots of the spectral density of some modes, $|\Phi_n(\mathbf{r}, z)|^2$, across the plane (ζ, z) for $n = 0, 1, 2, 3, 4, 5$.

Using the equality

$$J_n(t) = \frac{1}{2\pi} \int_0^{2\pi} e^{in\psi - it \sin \psi} d\psi, \quad (18)$$

after some manipulations the propagated modes take the following form:

$$\begin{aligned} \Phi_n(\mathbf{r}, z) &= \frac{2N_F}{r_0} \sqrt{\pi(n+1)} e^{ikz} (-i)^{n+1} \times e^{in\varphi} e^{i\pi N_F \rho^2} \\ &\times \int_0^1 J_n(2\pi N_F \rho u) e^{i\pi N_F u^2} u^{n+1} du, \end{aligned} \quad (19)$$

where the Fresnel number has been introduced as

$$N_F = \frac{kr_0^2}{2\pi z}, \quad (20)$$

together with the normalized transverse coordinate

$$\boldsymbol{\rho} = \frac{\mathbf{r}}{r_0} = (\zeta, \eta). \quad (21)$$

It is seen that the vortex structure of the phase is preserved during propagation and that, once the order n has been set, the propagated field depends only on the Fresnel number, as happens for the diffraction of a plane wave by a circular hole (corresponding to $n = 0$) [61]. Therefore, the Fresnel number will be taken as the natural variable

to represent the propagation distance. As examples, density plots of the spectral density of some modes across the plane (x, z) , that is, the squared modulus of the expression in equation (19), are shown in Figure 1.

As a first remark, we note that the property for a CSD of being uni-variable across a certain plane is not preserved during propagation. In fact, when modes propagate, their analytical forms actually change, and, in general, the product of the propagated modes, $\Phi_n(\mathbf{r}_1, z) \Phi_n^*(\mathbf{r}_2, z)$, is no longer proportional to $r_1^n r_2^n \exp[in(\varphi_1 - \varphi_2)]$, as it is required for the series to be interpreted as a power expansion.

Second, as also appears from Figure 1, the on-axis irradiance is zero for all modes, except $n = 0$. Furthermore, the modes spread during propagation at a rate that increases with n , giving less and less significant contributions in the central zone of the transverse planes. In particular, we expect that, when superpositions of modes are considered, only a finite number of modes need to be taken into account, which depends on the extent of the region where the field has to be evaluated. For example, modes with order 5 or higher can be safely neglected if the field has to be evaluated at $N_F = 0.5$ within a circular region of radius $2r_0$ (see Fig. 1).

3.2 Coherent modes in the far field

Unlike mode propagation in the Fresnel regime, far-field conditions lead to simple analytical forms. When the Fraunhofer conditions are met, the expression of a typical field

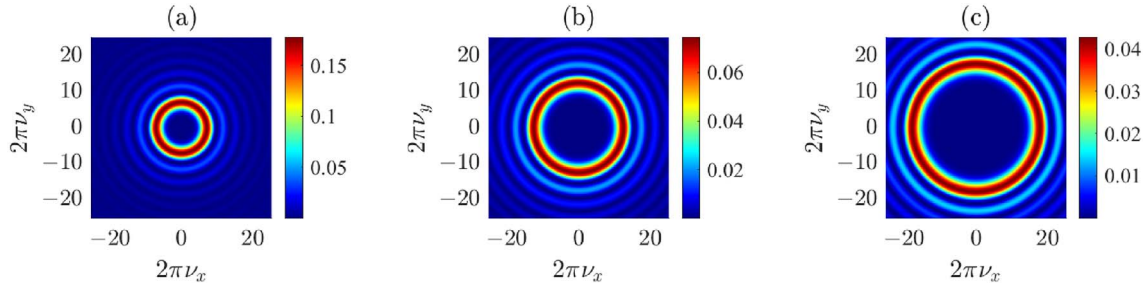


Fig. 2. Plots of the spectral density of the modes in the far field, equation (26) for $n = 5$ (a), 10 (b), 15 (c), with $r_0 = 1$.

(say, V_∞) is obtained from the Fourier transform, suitably scaled, of the field across the source [61]. For simplicity, the coordinate across the Fourier plane (say \mathbf{v}) will be taken as the spatial coordinate across a transverse plane in the far zone. Disregarding unessential proportionality factors and curvature terms, we simply write

$$V_\infty(\mathbf{v}) = \iint V(\mathbf{r}, 0) e^{-2\pi i \mathbf{v} \cdot \mathbf{r}} d\mathbf{r}, \quad (22)$$

the integral extending over the whole $z = 0$ plane.

Using polar coordinates, the above integral reads

$$V_\infty(\mathbf{v}) = \int_0^\infty \int_0^{2\pi} V(r, \varphi, 0) e^{-2\pi i v r \cos(\vartheta - \varphi)} r dr d\varphi, \quad (23)$$

with v and ϑ being the polar coordinates of \mathbf{v} . For the case of the modes in equation (7), the above integral gives

$$\begin{aligned} \Phi_{n,\infty}(\mathbf{v}) &= \frac{2(-i)^n}{r_0} \sqrt{\pi(n+1)} e^{in\vartheta} \\ &\times \int_0^{r_0} \left(\frac{r}{r_0}\right)^{n+1} J_n(2\pi v r) dr, \end{aligned} \quad (24)$$

J_n being the Bessel function of the first kind and order n [62]. Exploiting the following relation obeyed by the Bessel functions [63]:

$$\frac{d}{d\eta} [\eta^{n+1} J_{n+1}(\eta)] = \eta^{n+1} J_n(\eta), \quad (25)$$

the expression of the modes propagated in the far zone takes the simple form

$$\Phi_{n,\infty}(\mathbf{v}) = 2r_0 (-i)^n \sqrt{\pi(n+1)} e^{in\vartheta} \frac{J_{n+1}(2\pi r_0 v)}{2\pi r_0 v}. \quad (26)$$

Note that for $n = 0$ the latter equation gives rise to the well-known Fraunhofer diffraction pattern from a circular hole [61]. Indeed, for $n = 0$ the vortex field coincides with that of an ordinary plane wave. For $n \neq 0$, we can read equation (26) as the diffraction pattern produced by a vortex field that impinges on a circular aperture [48].

Plots of the spectral density of the propagated modes of equation (26) are given in Figure 2 for $n = 5, 10, 15$. It appears that, in general, the function is very small until its argument reaches values roughly equal to n , and then slowly goes to zero in an oscillating way.

In light of the above result, it is useful to express the CSD of a beam radiated by a uni-variable source through its Mercer expansion, which reads

$$\begin{aligned} W_\infty(\mathbf{v}_1, \mathbf{v}_2) &= 4\pi r_0^2 \sum_{n=0}^\infty \lambda_n (n+1) e^{in(\vartheta_1 - \vartheta_2)} \\ &\times \frac{J_{n+1}(2\pi r_0 v_1)}{2\pi r_0 v_1} \frac{J_{n+1}(2\pi r_0 v_2)}{2\pi r_0 v_2}. \end{aligned} \quad (27)$$

In some cases, this expression even leads to closed forms for the degree of coherence in the far field (μ_∞). This happens, for example, if $\lambda_n \propto (n+1)$ and we limit ourselves to point along radial directions (i.e., $\vartheta_1 = \vartheta_2$), in which case it can be shown that [64]

$$\mu_\infty(v_1, \vartheta, v_2, \vartheta) = 2 \frac{J_1(2\pi r_0(v_1 - v_2))}{2\pi r_0(v_1 - v_2)}. \quad (28)$$

4 sZegö and truncated sZegö sources

The first example of a uni-variable CSD we are going to show is that of the so-called *sZegö source*. The features of such a source across the source plane and in the far zone were studied and commented on in detail in a previous paper [38]. Here, we limit ourselves to recalling some of the main results obtained there. The effects of paraxial propagation of the radiated field will be studied here on the basis of the expression of the propagated modes obtained in Section 3.1. However, we find it convenient to perform such an analysis starting from a different uni-variable CSD, namely, the *truncated sZegö CSD*. Unlike *sZegö CSD*, in fact, the latter requires a finite number of modes and reduces to *sZegö CSD* when the number of modes goes to infinity. In such a way, the propagation features of the beams they radiate can be evaluated exactly through finite sums. However, we want to stress that a CSD of this type is interesting in itself because it is suitable to be synthesized in the laboratory starting from the superposition of a finite number of coherent fields [20, 28, 32, 37].

4.1 The sZegö source

To obtain a *sZegö CSD* we let $c_n = I_0(\nabla n)$ in equation (1), with I_0 a positive constant having dimensions of irradiance, so that

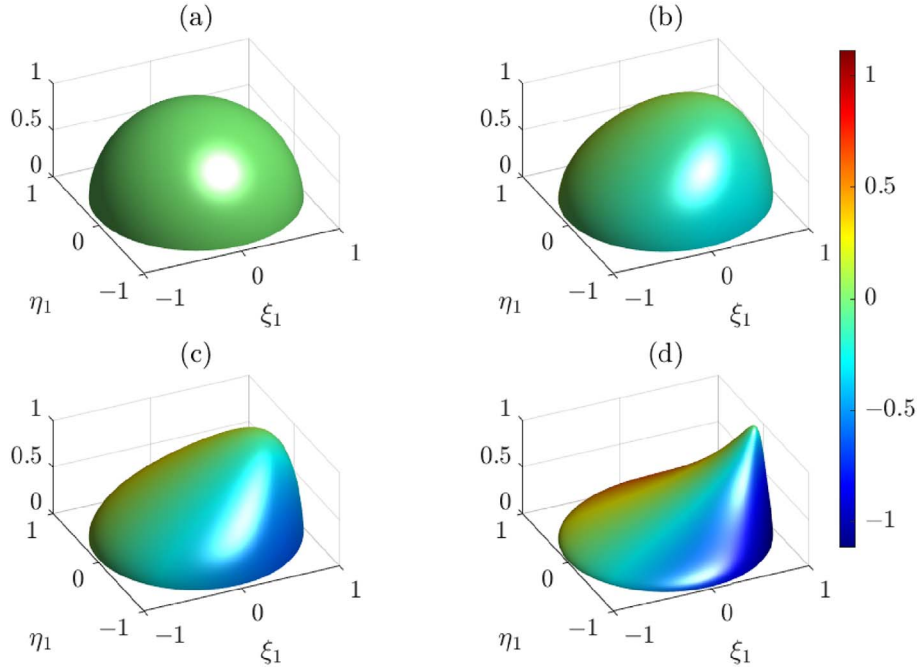


Fig. 3. Degree of coherence for a sZegö source at the source plane relative to a point located at (a) $\rho_2 = (0, 0)$; (b) $\rho_2 = (0.3, 0)$; (c) $\rho_2 = (0.6, 0)$; and (d) $\rho_2 = (0.9, 0)$. Absolute value is represented on the vertical axis, and the phase is coded in a color scale.

$$g(\zeta) = \frac{I_0}{1-\zeta} (|\zeta| < 1), \quad (29)$$

and the corresponding CSD turns out to be

$$W_S(\rho_1, \rho_2, 0) = \frac{I_0}{1 - \rho_1 \rho_2 e^{i(\varphi_1 - \varphi_2)}} \text{circ}(\rho_1) \text{circ}(\rho_2). \quad (30)$$

Spectral density and degree of coherence across the source plane turn out to be, from equations (15) and (16),

$$S_S(\rho, 0) = \frac{I_0}{1 - \rho^2} \text{circ}(\rho), \quad (31)$$

and

$$\mu_S(\rho_1, \rho_2, 0) = \frac{\sqrt{(1 - \rho_1^2)(1 - \rho_2^2)}}{1 - \rho_1 \rho_2 e^{i(\varphi_1 - \varphi_2)}} \text{circ}(\rho_1) \text{circ}(\rho_2), \quad (32)$$

respectively. It can be seen that the spectral density grows to infinity as ρ approaches one. This somewhat anomalous behavior has to be ascribed to the fact that an infinite number of modes contribute to the CSD of the source. It will be solved in the next subsection, where the series that gives rise to sZegö source will be truncated. Plots of μ_S (absolute value and phase) are shown in Figure 3 as a function of ρ_1 for fixed ρ_2 . The absolute value of μ_S is seen to vary from 1 (when $\rho_1 = \rho_2$) to 0 (along the circle $\rho_1 = 1$). Furthermore, when ρ_2 is in the center of the source, the phase is constant and equals to 0, while the range of variation of the phase increases with increasing ρ_2 . The presence of a coherence vortex can also be observed, which has charge -1 , centered at a point outside the source at a distance $1/\rho_2$ from the center [38].

The OAM degree of coherence at $z = 0$ can be derived using infinite geometric series. Together with the degree of orbitalization they take forms:

$$o_S(\rho_1, \rho_2, 0) = \sqrt{\frac{(1 - \rho_1^2)(1 - \rho_2^2)}{1 - \rho_1^2 \rho_2^2}},$$

$$O_S(\rho, 0) = (1 - \rho^2)^2. \quad (33)$$

Note that $O_S(\rho, 0)$ has a particularly simple form since for this source $\lambda_n(\rho, 0) \geq \lambda_{n+1}(\rho, 0)$ for all n and ρ , which is not generally true for other source classes. The color density plot of the OAM degree of coherence for this beam is shown in Figure 4a. As expected, this quantity takes the unity value at $\rho_1 = \rho_2 = 0$ but gradually decreases and reaches zero for $\rho_1 = 1$ or $\rho_2 = 1$. We also note that it is not generally unity at the coinciding radii $\rho_1 = \rho_2 \neq 0$, unlike the classic degree of coherence that would be at the coinciding points.

An explicit expression of the CSD of the field radiated in the far zone, $W_{S,\infty}$, can hardly be derived directly from the CSD in $z = 0$, but from its modal expansion, with the modes of equation (26) and the eigenvalues given by

$$\lambda_n = I_0 \frac{\pi r_0^2}{n+1}, \quad (n = 0, 1, \dots), \quad (34)$$

takes the form

$$W_{S,\infty}(\mathbf{v}_1, \mathbf{v}_2) \propto \sum_{n=0}^{\infty} \frac{J_{n+1}(2\pi r_0 v_1)}{2\pi r_0 v_1} \times \frac{J_{n+1}(2\pi r_0 v_2)}{2\pi r_0 v_2} e^{in(\vartheta_1 - \vartheta_2)}, \quad (35)$$

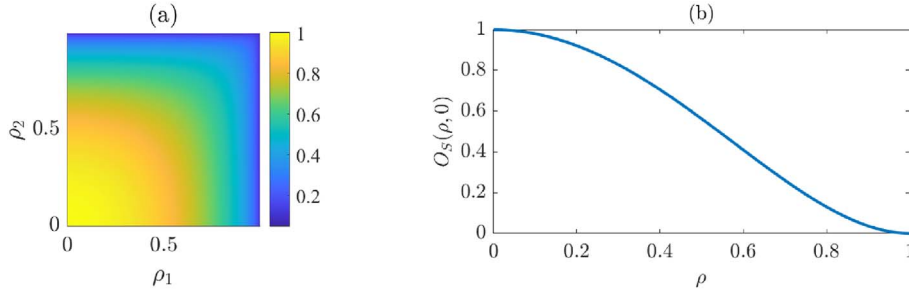


Fig. 4. (a) OAM degree of coherence $o_S(\rho_1, \rho_2)$ and (b) degree of orbitalization $O_S(\rho)$ for a sZegö source.

which can be used to evaluate $S_{S,\infty}$ and $\mu_{S,\infty}$ numerically. The latter quantities, evaluated by adding the contribution of the first 100 modes, are shown in Figures 5 and 6, respectively.

For the case of the spectral density, it was found that there are no significant differences, at least in the range $r_0\nu < 1$, when calculating it using only the first 6 modes or the first 100 modes, so that the contribution of modes of order higher than 6 turns out to be negligible. Basically, the same conclusions hold for the degree of coherence, but in such a case, the first 10 modes have to be considered. The degree of coherence shows cylindrical symmetry when calculated in relation to the beam axis, with its absolute value reaching a maximum at the center of the beam and showing decreasing oscillations, while the phase alternates between 0 and π . When evaluated in relation to a direction outside the axis, the oscillations of the absolute value of the DOC are distorted, and the phase varies gradually. In this case also the presence of coherence vortices can be observed (with charge +1 and -1), corresponding to the zeros of $\mu_{S,\infty}$ [38]. The absolute value is represented on the vertical axis, and the phase is coded in a color scale. The first 100 modes were considered in the calculation.

The far-zone OAM degree of coherence of a field radiated by a sZegö source takes form

$$o_S(v_1, v_2) = \frac{2\sqrt{\sum_{n=0}^{\infty} J_{n+1}^2(2\pi r_0 v_1) J_{n+1}^2(2\pi r_0 v_2)}}{\sqrt{1 - J_0^2(2\pi r_0 v_1)} \sqrt{1 - J_0^2(2\pi r_0 v_2)}}, \quad (36)$$

after using a summation formula for $J_{n+1}^2(2\pi r_0 v_j)$, $j = 1, 2$ in the denominator. Figure 7a shows this quantity as a function of v_1, v_2 with $r_0 = 1$, where we restrict ourselves to a region close to the axis. This distribution is structurally different from that in Figure 4a, since the coherence no longer decreases monotonically with the increasing radii but oscillates between wider and narrower distributions. It should also be noted that for $v_1 = v_2 = v$ the OAM coherence remains fairly high within the plotted region around the axis.

The degree of orbitalization becomes

$$O_S(v) = 2 \frac{J_p^2(2\pi r_0 v) - J_q^2(2\pi r_0 v)}{1 - J_0^2(2\pi r_0 v)}, \quad (37)$$

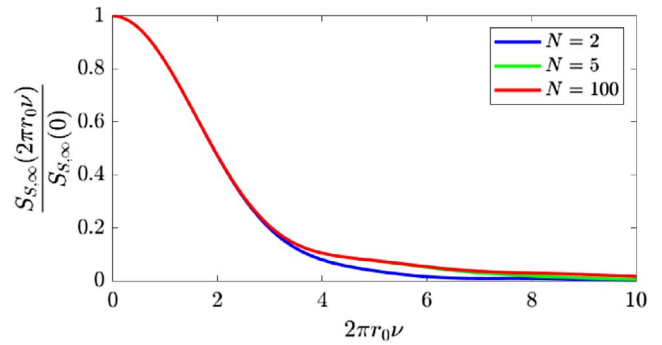


Fig. 5. Spectral density for a sZegö source in the far field (with $r_0 = 1$), calculated by adding the first 2, 5, and 100 modes, respectively.

where p and q are the indices of the largest and the second largest eigenvalues σ_n for a given radius v . We note that unlike in the source plane, where the zeroth and the first eigenvalues are the largest and second largest for all radii, in the far field such eigenvalues must be determined numerically. Figure 7b shows the degree of orbitalization as a function of v , with $r_0 = 1$, for $v \leq 1$. Unlike in the source plane, where this degree monotonically decreases from unity to zero, see Figure 4b, it shows a piecewise-continuous profile without smoothness at junctions. This is due to the fact that many OAM modes are competing for being the maximum and the second maximum. For example, close to the axis, modes $n = 0$ and $n = 1$ constitute this pair, but at $v \approx 0.419$, modes $n = 1$ and $n = 2$ become such. Hence, most of the oscillations are due to switching to higher indexes, with one exception: in the region $0.817 \leq v \leq 0.894$, the $n = 0$ mode has a crest becoming the second largest eigenvalue again.

4.2 Truncated sZegö sources

In this case, we let $c_n = I_0$ if $0 \leq n < N$ and $c_n = 0$ if $n \geq N$, so that equation (1) gives

$$g_T(\zeta) = I_0 \sum_{n=0}^{N-1} \zeta^n = I_0 \frac{1 - \zeta^N}{1 - \zeta} \quad (|\zeta| < 1), \quad (38)$$

and the corresponding CDS turns out to be

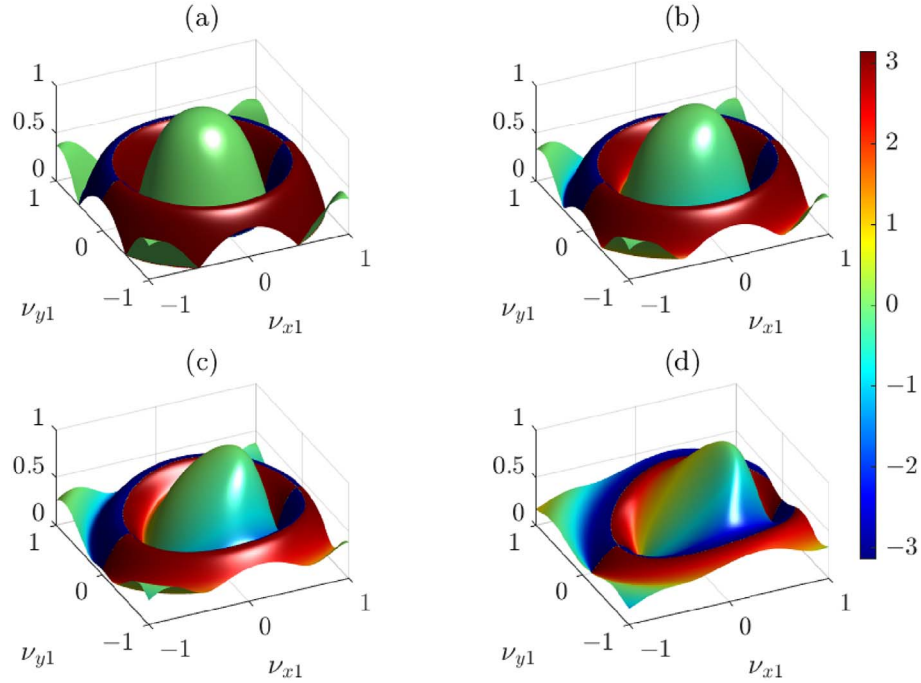


Fig. 6. Degree of coherence for a sZegő source across a plane in the far zone relative to a point located at (a) $\mathbf{v}_2 = (0, 0)$; (b) $\mathbf{v}_2 = (0.16, 0)$; (c) $\mathbf{v}_2 = (0.32, 0)$; and (d) $\mathbf{v}_2 = (0.48, 0)$. Absolute value is represented on the vertical axis, and the phase is coded in a color scale. The first 100 modes were considered in the calculation.

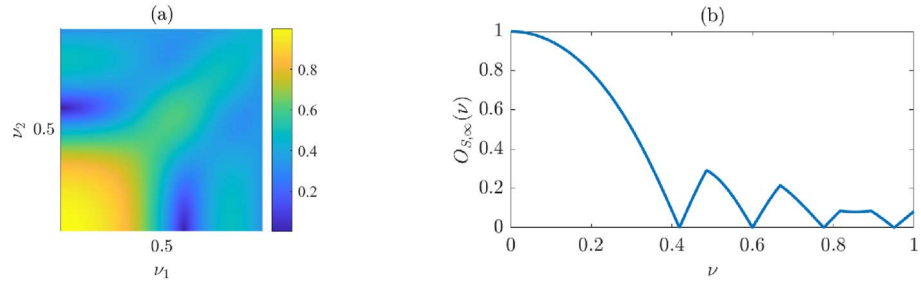


Fig. 7. (a) OAM degree of coherence $o_S(v_1, v_2)$; (b) degree of orbitalization $O_S(v)$ for a far field radiated by sZegő source.

$$W_T(\boldsymbol{\rho}_1, \boldsymbol{\rho}_2, 0) = I_0 \frac{1 - (\rho_1 \rho_2)^N e^{iN(\varphi_1 - \varphi_2)}}{1 - \rho_1 \rho_2 e^{i(\varphi_1 - \varphi_2)}}; \quad (39)$$

$$(0 \leq \rho_1, \rho_2 < 1).$$

Spectral density and degree of coherence across the source plane turn out to be, from equations (15) and (16),

$$S_T(\boldsymbol{\rho}, 0) = I_0 \frac{1 - \rho^{2N}}{1 - \rho^2} \text{circ}(\rho), \quad (40)$$

and

$$\begin{aligned} \mu_T(\boldsymbol{\rho}_1, \boldsymbol{\rho}_2, 0) &= \sqrt{\frac{(1 - \rho_1^2)(1 - \rho_2^2)}{(1 - \rho_1^{2N})(1 - \rho_2^{2N})}} \\ &\times \frac{1 - (\rho_1 \rho_2)^N e^{iN(\varphi_1 - \varphi_2)}}{1 - \rho_1 \rho_2 e^{i(\varphi_1 - \varphi_2)}} \text{circ}(\rho_1) \text{circ}(\rho_2), \end{aligned} \quad (41)$$

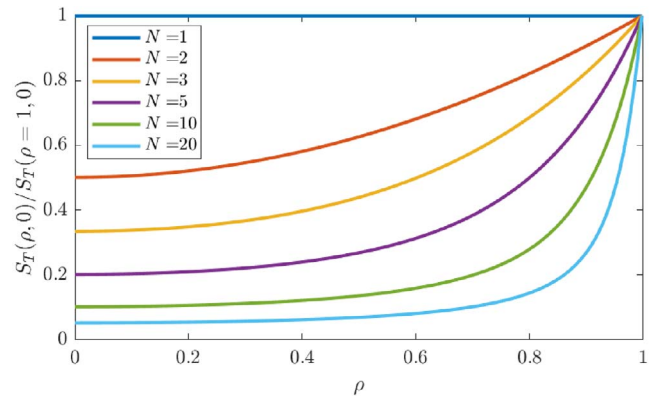


Fig. 8. Spectral density at the source (normalized to the maximum) for a truncated sZegő CSD with $N = 1, 2, 3, 5, 10, 20$.

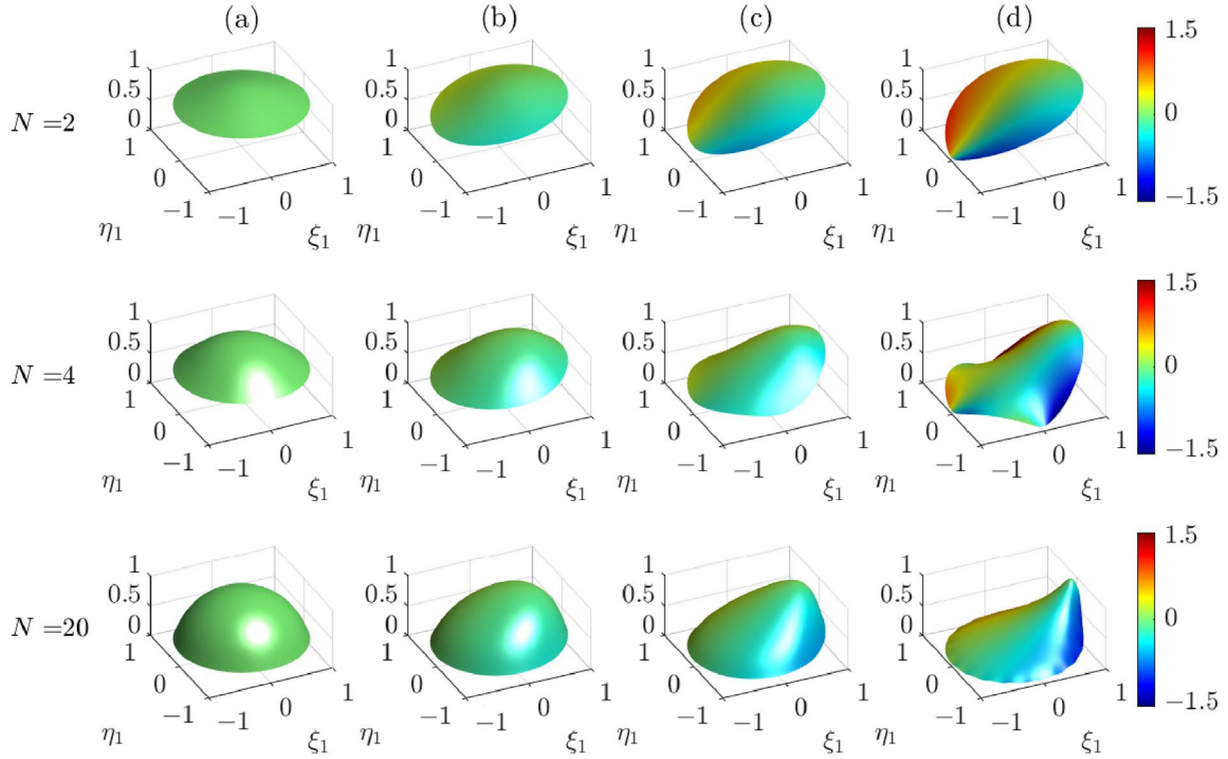


Fig. 9. Degree of coherence at the source plane, for a truncated sZegö CSD with $N = 2, 4, 20$ (from top to bottom), relative to a point located at (a) $\rho_2 = (0, 0)$; (b) $\rho_2 = (0.3, 0)$; (c) $\rho_2 = (0.6, 0)$; and (d) $\rho_2 = (0.9, 0)$. Absolute value is represented on the vertical axis, and the phase is coded in a color scale.

respectively. The plots of S_T and μ_T are shown in [Figures 8 and 9](#), respectively. It can be seen that, as the number of modes increases, the spectral density becomes more and more similar to that of the sZegö source but never diverges, as expected. On the other hand, the DOC is highly dependent on the number of modes considered.

Two aspects deserve to be noticed. First, the coherence area decreases as N increases, as expected. The second aspect concerns the phase structure of μ_T . It can be highlighted in a simpler way if we focus our attention on the second fraction in equation (41), provided the other terms are positive. Using again the variable $\zeta = \rho_1 \rho_2 \exp[i(\varphi_1 - \varphi_2)]$, this term can be written as

$$\frac{1 - \zeta^N}{1 - \zeta} = - \frac{\prod_{n=1}^N (\zeta - \zeta_n)}{1 - \zeta}, \quad (42)$$

where ζ_n ($n = 1, \dots, N$) are the solutions of the equation $\zeta^N = 1$, namely, $\zeta_n = \exp(i2\pi n/N)$. Therefore, since $\zeta_N = 1$, we have

$$- \frac{\prod_{n=1}^N (\zeta - \zeta_n)}{1 - \zeta} = \prod_{n=1}^{N-1} (\zeta - \zeta_n), \quad (43)$$

which for fixed values of ρ_2 and φ_2 can be written as

$$\prod_{n=1}^{N-1} (\zeta - \zeta_n) = \rho_2^{(N-1)} e^{-i(N-1)\varphi_2} \times \prod_{n=1}^{N-1} \left[\rho_1 e^{i\varphi_1} - \frac{1}{\rho_2} e^{i(\varphi_2 + 2\pi n/N)} \right], \quad (44)$$

representing the product of $N - 1$ vortices, each having charge $+1$, centered on $N - 1$ vertices of a regular enneagon, at a distance $1/\rho_2$ from the center.

To better understand this point, let us take $\varphi_2 = 0$. Then, the n th term of the product takes the form

$$\rho_1 e^{i\varphi_1} - \frac{1}{\rho_2} e^{i2\pi n/N} = \left[\zeta_1 - \frac{1}{\rho_2} \cos\left(\frac{2\pi n}{N}\right) \right] + i \left[\eta_1 - \frac{1}{\rho_2} \sin\left(\frac{2\pi n}{N}\right) \right], \quad (45)$$

which actually represents a vortex with charge $+1$ and center at

$$\rho_1^{(n)} = \left(\frac{1}{\rho_2} \cos\left(\frac{2\pi n}{N}\right), \frac{1}{\rho_2} \sin\left(\frac{2\pi n}{N}\right) \right). \quad (46)$$

The phase structure of the DOC is shown in [Figure 10](#) for $\rho_2 = (0.9, 0)$ and several values of N .

The OAM degree of coherence for this source at $z = 0$ can be derived using finite geometric series. This quantity and the degree of orbitalization take form

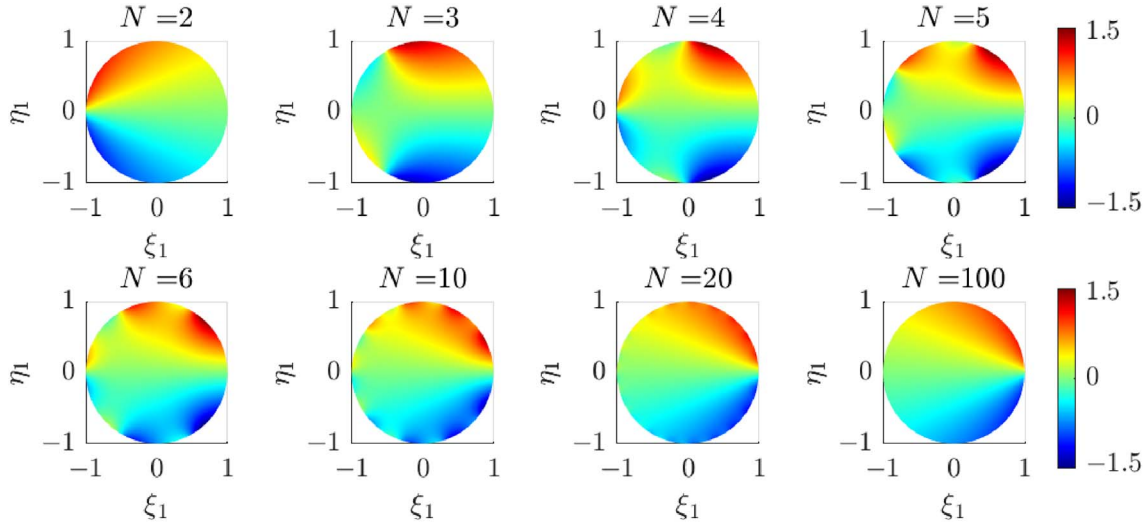


Fig. 10. Phase of the degree of coherence at the source plane, for a truncated sZegö CSD relative to the point $\rho_2 = (0.9, 0)$ for several values of N .

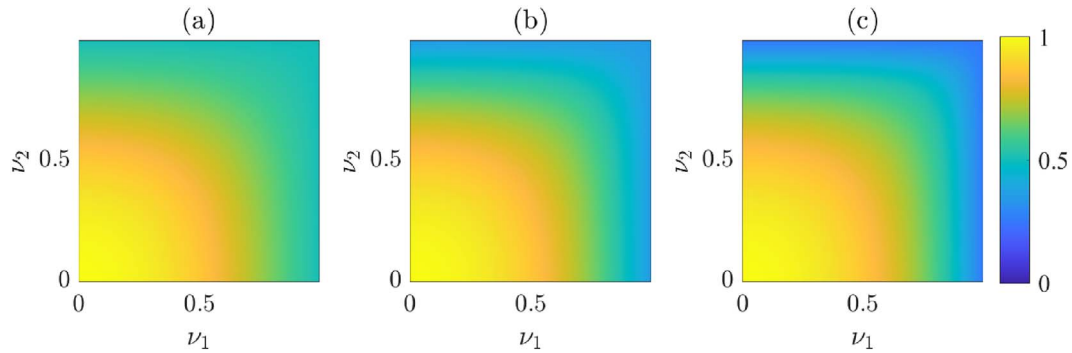


Fig. 11. OAM degree of coherence $o_T(\rho_1, \rho_2)$ for truncated sZegö sources with (a) $N = 4$; (b) $N = 8$; (c) $N = 16$.

$$\begin{aligned}
 o_T(\rho_1, \rho_2, 0) &= \sqrt{\frac{(1 - \rho_1^2)(1 - \rho_2^2)}{1 - \rho_1^2 \rho_2^2}} \\
 &\quad \times \sqrt{\frac{1 - \rho_1^{2N} \rho_2^{2N}}{(1 - \rho_1^{2N})(1 - \rho_2^{2N})}}; \\
 O_T(\rho, 0) &= \frac{(1 - \rho^2)^2}{1 - \rho^{2N}}. \quad (47)
 \end{aligned}$$

The plots of the OAM degree of coherence for this source are shown in [Figures 11a–11c](#), for several values of N . Unlike for the sZegö sources the distributions do not decrease to zero for $\rho_1 = 1$ or $\rho_2 = 1$ but rather take on values in the interval $(0, 1)$ decreasing with increasing N . The plots of the degree of orbitalization are shown in [Figure 12](#) for several values of N . The case $N = \infty$ is also shown corresponding to the un-truncated sZegö source. While all the curves have monotonic behavior taking on unit value at $\rho = 0$ and decreasing to zero at $\rho = 1$ only the curve for $N = 1$ is convex on the whole interval, all the others change convexity once.

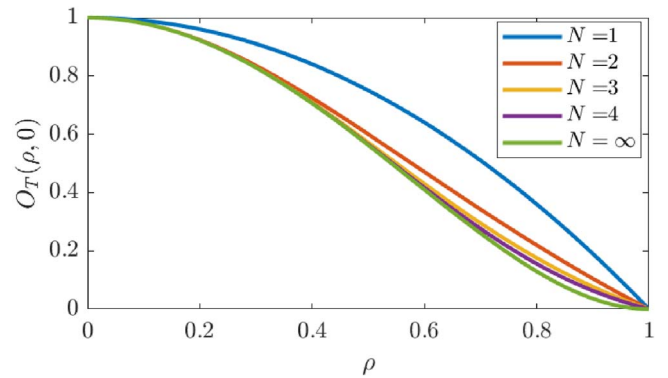


Fig. 12. Degree of orbitalization $O_T(\rho)$ for truncated sZegö sources with different values of N . The case $N = \infty$ corresponds to the non-truncated sZegö source.

To evaluate the propagated CSD in the near and in the far field equations (14) and (19), or (26) are used. Equations (38) and (8) give, for the eigenvalues,

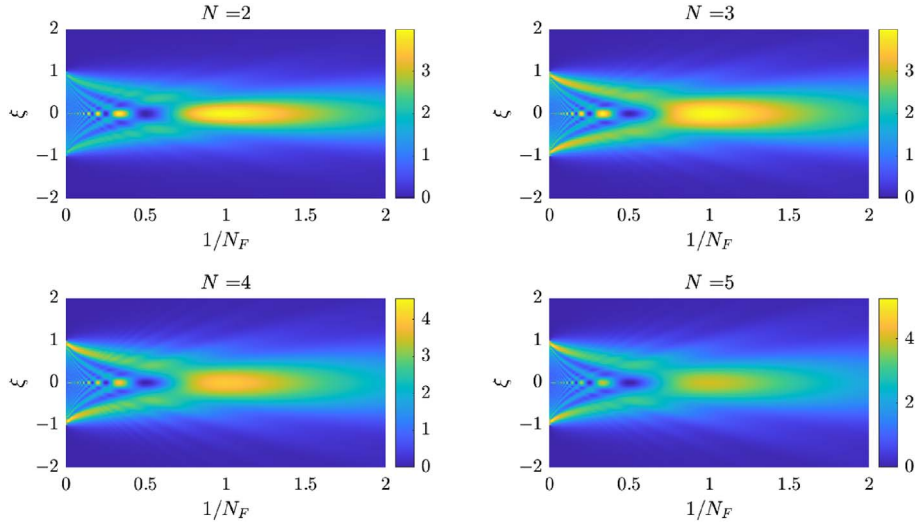


Fig. 13. Spectral density versus the inverse of the Fresnel number for several truncated sZegö sources with N modes.

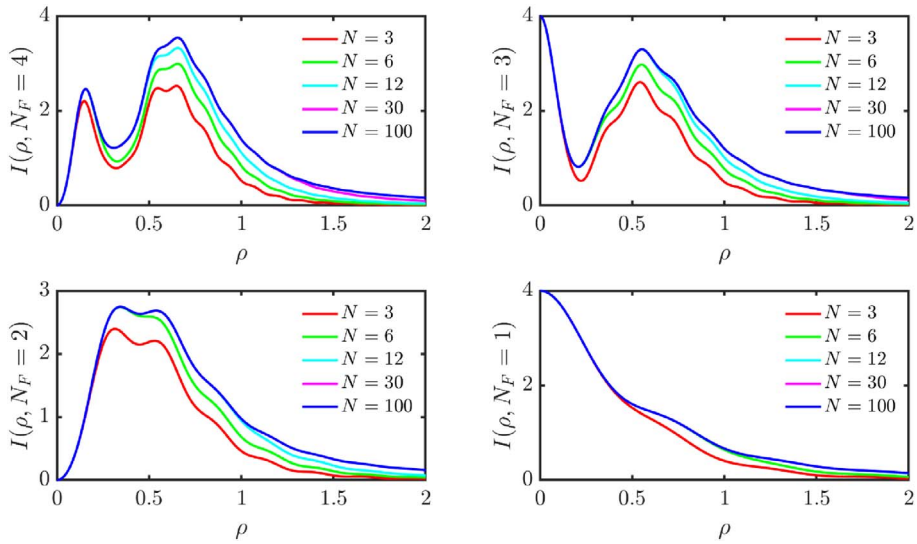


Fig. 14. Spectral density versus the inverse of the Fresnel number for different truncated sZegö sources.

$$\lambda_n = \begin{cases} I_0 \frac{\pi r_0^2}{n+1} & (0 \leq n < N); \\ 0 & (n \geq N). \end{cases} \quad (48)$$

Figure 13 shows examples of the spectral density, across the (x, z) plane, of the field propagated from sZegö sources of various orders. It can be observed that the main contribution for large propagation distances is due to the 0 th order mode (compare Fig. 13 with Fig. 1 for $n = 0$).

As commented above, the addition of more and more modes modifies the distribution of the spectral density only for small propagation distances. This is confirmed by the plots in Figure 14 where the spectral density profiles are calculated at several propagation distances for sZegö truncated sources with different numbers of modes. For a Fresnel number $N_F = 4$, the five profiles are different, although those corresponding to $N = 30$ and $N = 100$ are

practically the same up to a normalized distance $\rho = 1$. For $N_F = 1$ the profiles practically coincide for all truncated sZegö sources with $N \geq 12$. This profile should be the same as the one for sZegö source.

The same approach can be used to evaluate the degree of coherence across different planes (Fig. 15). The analogous calculations across the source plane and in the far field [38] showed the presence of coherence vortices (in both cases).

The far-zone OAM degree of coherence radiated by a truncated sZegö source takes the form

$$o_T(v_1, v_2) = \frac{\sqrt{\sum_{n=0}^{N-1} J_{n+1}^2(2\pi r_0 v_1) J_{n+1}^2(2\pi r_0 v_2)}}{\prod_{j=1,2} \sqrt{\sum_{n=0}^{N-1} J_{n+1}^2(2\pi r_0 v_j)}}. \quad (49)$$

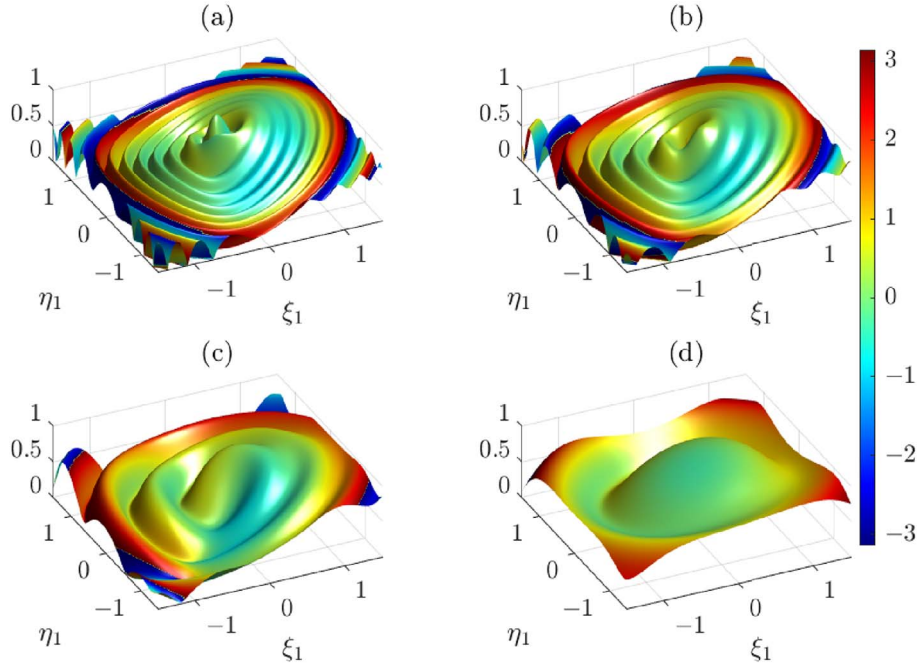


Fig. 15. Degree of coherence relative to a point located at $\rho_2 = (0, 0.5)$ for a truncated sZegö source with $N = 4$ at several propagation distances (a) $N_F = 3$; (b) $N_F = 2$; (c) $N_F = 1$; (d) $N_F = 0.5$. The absolute value is represented on the vertical axis, and the phase is coded in a color scale.

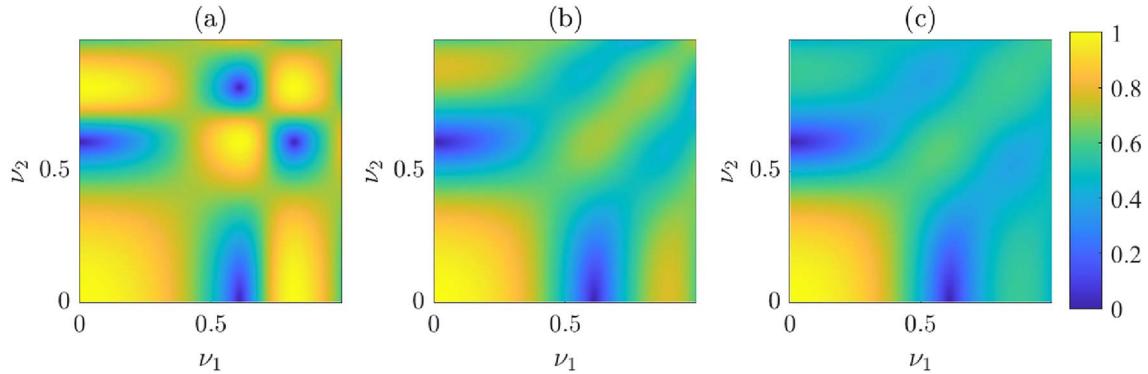


Fig. 16. OAM degree of coherence $o_T(v_1, v_2)$ for truncated sZegö far fields with (a) $N = 2$; (b) $N = 3$; (c) $N = 4$.

Figure 16 shows this quantity for several values of the summation index: (a) $N = 2$, (b) $N = 3$, and (c) $N = 4$. As N increases, the distributions start resembling that for the non-truncated model, if compared to Figure 7a. This practically occurs already for $N = 4$, as higher-order modes deliver much smaller contributions to the sums.

For truncated sZegö far fields the degree of orbitalization becomes

$$O_T(\mathbf{v}) = \frac{J_p^2(2\pi r_0 v) - J_q^2(2\pi r_0 v)}{\sum_{n=0}^{N-1} J_{n+1}^2(2\pi r_0 v)}, \quad (50)$$

where, as above, p and q are the indices of the largest and the second largest eigenvalues. Analogously to the non-truncated model, the determination of the largest and

the second largest eigenvalues for different radii was carried out numerically.

Figure 17 shows formation of the degree of orbitalization for (a) $N = 2$ and (b) $N = 3$. For $N = 2$ the degree exhibits strictly oscillatory nature with smooth maxima and non-smooth minima, all at zeroes. This is due to the fact that only two modes compete with each other for being maximum and second maximum and can only alternate. This behavior is similar to that of the degree of polarization, also involving competition of two electric field components. Starting from $N = 3$ both maxima and minima are not smooth, since the switches are determined by three pairs of modes. Figure 17c summarizes the behavior for cases $N = 2$, $N = 3$ and $N \rightarrow \infty$ (non-truncated model), same as in Figure 7b. In parts where the curves are almost the same, the same modes act as the largest and second largest

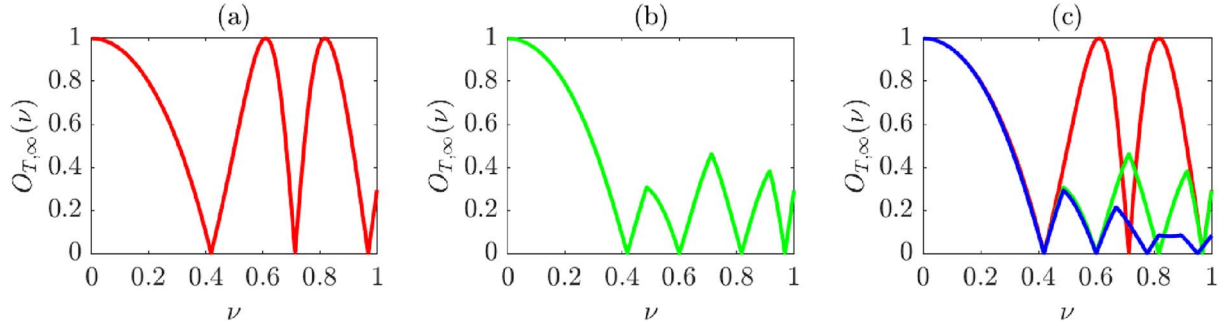


Fig. 17. Degree of orbitalization $O_T(\nu)$ for truncated sZegő far fields with (a) $N = 2$; (b) $N = 3$; (c) combination of $N = 2$, $N = 3$, and non-truncated model.

eigenvalues resulting in the same numerator in equation (17), while the denominator has an increasing value with increasing N . This always occurs at small ν as the 0th mode always dominates close to the axis.

5 Further examples of uni-variable sources

Different uni-variable CSDs can be defined by choosing different sets of c_n coefficients, and in many cases they are given in closed form, as happened for the case in the previous section. Actually, using handbooks of mathematical formulas, dozens of other CSDs can be defined from formulas involving power series. Some of them lead to closed forms even when the series is truncated. This is particularly useful because, as we saw for sZegő and truncated sZegő sources, in such a case the effects of truncation can be evaluated quite simply. Furthermore, in any practical realization of partially coherent sources based on the superimposition of perfectly coherent and mutually uncorrelated fields, the number of modes must be necessarily truncated.

Among others, we quote the following (formula 5.2.2.4 of [64]):

$$g(\zeta) = I_0 \sum_{n=1}^{\infty} n \zeta^n = I_0 \frac{\zeta}{(1-\zeta)^2}, \quad (51)$$

together with its truncated version (formula 4.1.7.2 of [64])

$$g_T(\zeta) = I_0 \sum_{n=1}^N n \zeta^n = I_0 \frac{\zeta + (N\zeta - N - 1)\zeta^{N+1}}{(1-\zeta)^2}, \quad (52)$$

with integer N .

Another interesting example of a source obtained with a finite number of modes is that of the *binomial source*, for which (formula 4.2.3.1 of [64])

$$g(\zeta) = I_0 \sum_{n=0}^N \binom{N}{n} \zeta^n = I_0 (1 + \zeta)^N. \quad (53)$$

As a last example, we quote the following, which will be discussed in a little more detail. If we take (formula 5.2.7.2 of [64])

$$g(\zeta) = I_0 \sum_{n=0}^{\infty} \frac{(\gamma^2 \zeta)^n}{n!} = I_0 e^{\gamma^2 \zeta}, \quad (54)$$

with γ^2 a positive dimensionless parameter, the corresponding uni-variable CSD turns out to be

$$W_G(\boldsymbol{\rho}_1, \boldsymbol{\rho}_2) = I_0 \exp \{ \gamma^2 \boldsymbol{\rho}_1 \boldsymbol{\rho}_2 \exp [i(\varphi_1 - \varphi_2)] \} \text{circ}(\rho_1) \text{circ}(\rho_2), \quad (55)$$

and the corresponding spectral density has the form

$$S_G(\rho) = I_0 e^{\gamma^2 \rho^2} \text{circ}(\rho). \quad (56)$$

The interest in such sources comes from what follows. If we express W_G through the vectors $\boldsymbol{\rho}_1$ and $\boldsymbol{\rho}_2$, since $\boldsymbol{\rho}_j = (\xi_j, \eta_j)$ and $\boldsymbol{\rho}_j \exp(i\varphi_j) = \xi_j + i\eta_j$, ($j = 1, 2$), equation (55) can also be written as

$$\begin{aligned} W_G(\boldsymbol{\rho}_1, \boldsymbol{\rho}_2) &= I_0 e^{i\gamma^2(\xi_1 \xi_2 + \eta_1 \eta_2)} e^{-i\gamma^2(\xi_1 \eta_2 - \xi_2 \eta_1)} \text{circ}(\rho_1) \text{circ}(\rho_2) \\ &= I_0 e^{i\gamma^2 \boldsymbol{\rho}_1 \cdot \boldsymbol{\rho}_2} e^{-i\gamma^2 (\boldsymbol{\rho}_1 \times \boldsymbol{\rho}_2)_z} \text{circ}(\rho_1) \text{circ}(\rho_2) \end{aligned} \quad (57)$$

or, after some manipulations,

$$\begin{aligned} W_G(\boldsymbol{\rho}_1, \boldsymbol{\rho}_2) &= I_0 e^{i\gamma^2(\rho_1^2 + \rho_2^2)/2} e^{-i\gamma^2 |\boldsymbol{\rho}_1 - \boldsymbol{\rho}_2|^2 / 2} e^{-i\gamma^2 (\boldsymbol{\rho}_1 \times \boldsymbol{\rho}_2)_z} \text{circ}(\rho_1) \text{circ}(\rho_2), \end{aligned} \quad (58)$$

which apparently has the form of a twisted Gaussian Schell-model source with saturated twist [40], the only difference being the sign in the argument of the Gaussian amplitude term. In particular, the degree of coherence turns out to be

$$\mu_G(\boldsymbol{\rho}_1, \boldsymbol{\rho}_2) = e^{-\gamma^2 |\boldsymbol{\rho}_1 - \boldsymbol{\rho}_2|^2 / 2} e^{-i\gamma^2 (\boldsymbol{\rho}_1 \times \boldsymbol{\rho}_2)_z} \text{circ}(\rho_1) \text{circ}(\rho_2), \quad (59)$$

whose modulus is

$$|\mu_G(\boldsymbol{\rho}_1, \boldsymbol{\rho}_2)| = e^{-\gamma^2 |\boldsymbol{\rho}_1 - \boldsymbol{\rho}_2|^2 / 2} \text{circ}(\rho_1) \text{circ}(\rho_2). \quad (60)$$

The eigenvalues of the Mercer expansion of W_G turn out to be

$$\lambda_n = I_0 \gamma^{2n} \frac{\pi r_0^2}{(n+1)!}, \quad (61)$$

from which the propagation features of the radiated beams could be evaluated.

In this case, too, the truncated version of the series can be expressed in closed form because (formula 4.1.7.10 of [64])

$$g_T(\zeta) = I_0 \sum_{n=0}^N \frac{(\gamma^2 \zeta)^n}{n!} = I_0 \frac{\Gamma(N+1, \gamma^2 \zeta)}{N!} e^{\gamma^2 \zeta}, \quad (62)$$

where $\Gamma(\cdot, \cdot)$ is the incomplete Gamma function [63].

6 Conclusions

Uni-variable CSDs can be derived from any function of a single complex argument whose Taylor series involves only non-negative coefficients. The convergence range of the series determines the spatial extent of the source. The Taylor series can be directly related to the Mercer expansion of the CSD of the source in such a way that the coherent modes turn out to be optical vortices, restricted to a circle at the source plane, and the corresponding eigenvalues are proportional to the Taylor coefficients.

Although the coherence features of light across the source plane can be directly derived from the analytical form of the CSD, the analogous properties for the radiated beam can hardly be evaluated in closed form. Nevertheless, from the knowledge of modes and eigenvalues of the CSD across the source, the coherence features of the radiated beam can be evaluated both in the Fresnel regime and in the Fraunhofer regime.

In this paper, the tools for studying the properties of the propagated field have been provided and applied to a test case, that is, the sZegö source. Furthermore, the effects, on the coherence properties of the source and the radiated field, of truncating the Taylor series have also been investigated. This is crucial from an experimental point of view, because limiting the Taylor series (i.e., the coherent-mode expansion of the CSD) to a finite number of terms becomes necessary whenever sources of this kind have to be synthesized through the superposition of mutually uncorrelated perfectly coherent fields.

Since the coherent modes of uni-variable CSDs possess vortex-like structures at various OAM indices, the overall fields can be regarded as carrying OAM in multiple states. Hence, besides the spectral density and the degree of coherence, which carry information about correlations in the physical space, some recently introduced measures, namely, the OAM degree of coherence and the degree of orbitalization, have also been invoked to characterize the radial correlations of the investigated sources in the OAM space, i.e., the polar Fourier space. Although the technique presented here has been applied to the sZegö CSD and to its truncated version (the truncated sZegö CSD), it can be applied to any source of the uni-variable type. The number of uni-variable CSD that can be envisaged starting from the Taylor expansion of a single-argument function is actually huge, and this work lays the foundation for the design and tailoring of sources with required coherence characteristics, both on the source plane and in propagation.

Funding

This work has been supported by the Spanish Ministerio de Economía y Competitividad under project PID2023-148021NB-I00 and Project FASLIGTH (RED2022-134391-T).

Conflicts of interest

This work has no financial or non-financial competing interests.

Data availability statement

Data will be made available on request.

Author contribution statement

All authors have contributed equally to all aspects of this work, including conceptualization, methodology, formal analysis, and the writing of the original draft and final manuscript.

References

- 1 Yu J, Zhu X, Wang F, Chen Y, Cai Y, Research progress on manipulating spatial coherence structure of light beam and its applications, *Prog. Quantum Electron.* **91–92**, 100486 (2023). <https://doi.org/10.1016/j.pquantelec.2023.100486>.
- 2 Rosales-Guzmán C, Rodríguez-Fajardo V, A perspective on structured light's applications, *Appl. Phys. Lett.* **125**, 200503 (2024). <https://doi.org/10.1063/5.0236477>.
- 3 Liang C, Wu G, Wang F, Li W, Cai Y, Ponomarenko SA, Overcoming the classical Rayleigh diffraction limit by controlling two-point correlations of partially coherent light sources, *Opt. Express* **25**, 28352 (2017). <https://doi.org/10.1364/OE.25.028352>.
- 4 Shen Y, Sun H, Peng D, Chen Y, Cai Q, Wu D, Wang F, Cai Y, Ponomarenko SA, Optical image reconstruction in 4f imaging system: Role of spatial coherence structure engineering, *Appl. Phys. Lett.* **118**, 181102 (2021). <https://doi.org/10.1063/5.0046288>.
- 5 Gibson G, Courtial J, Padgett MJ, Vasnetsov M, Pas'ko V, Barnett SM, Franke-Arnold S, Free-space information transfer using light beams carrying orbital angular momentum, *Opt. Express* **12**, 5448 (2004). <https://doi.org/10.1364/OPEX.12.005448>.
- 6 Wang J, et al., Terabit free-space data transmission employing orbital angular momentum multiplexing, *Nat. Photonics* **6**, 488 (2012). <https://doi.org/10.1038/nphoton.2012.138>.
- 7 Liu X, Shen Y, Liu L, Wang F, Cai Y, Experimental demonstration of vortex phase-induced reduction in scintillation of a partially coherent beam, *Opt. Lett.* **38**, 5323 (2013). <https://doi.org/10.1364/OL.38.005323>.
- 8 Gbur G, Partially coherent beam propagation in atmospheric turbulence, *J. Opt. Soc. Am. A* **31**, 2038 (2014). <https://doi.org/10.1364/JOSAA.31.002038>.
- 9 Lin S, Zhu X, Shen Y, Wang F, Chen X, Gbur G, Cai Y, Yu J, Statistically stationary random light for high-security encryption, *Optica* **12**, 1261 (2025). <https://doi.org/10.1364/OPTICA.546899>.
- 10 Zhao C, Cai Y, Trapping two types of particles using a focused partially coherent elegant Laguerre–Gaussian beam, *Opt. Lett.* **36**, 2251 (2011). <https://doi.org/10.1364/OL.36.002251>.

- 11 Zhang Z, Liu X, Wang H, Liang C, Cai Y, Zeng J, Flexible optical trapping and manipulating Rayleigh particles via the cross-phase modulated partially coherent vortex beams, *Opt. Express* **32**, 35051 (2024). <https://doi.org/10.1364/OE.539069>.
- 12 Guo J, Ming S, Wu Y, Chen LQ, Zhang W, Super-sensitive rotation measurement with an orbital angular momentum atom-light hybrid interferometer, *Opt. Express* **29**, 208 (2021). <https://doi.org/10.1364/OE.409964>.
- 13 Gori F, Santarsiero M, Devising genuine spatial correlation functions, *Opt. Lett.* **32**, 3531 (2007). <https://doi.org/10.1364/OL.32.003531>.
- 14 Martínez-Herrero R, Mejías PM, Gori F, Genuine cross-spectral densities and pseudo-modal expansions, *Opt. Lett.* **34**, 1399 (2009). <https://doi.org/10.1364/OL.34.001399>.
- 15 Raghunathan SB, van Dijk T, Peterman EJG, Visser TD, Experimental demonstration of an intensity minimum at the focus of a laser beam created by spatial coherence: application to the optical trapping of dielectric particles, *Opt. Lett.* **35**, 4166 (2010). <https://doi.org/10.1364/OL.35.004166>.
- 16 Gbur G, Visser TD, The structure of partially coherent fields, *Prog. Opt.* **55**, 285 (2010). <https://doi.org/10.1016/B978-0-444-53705-8.00005-9>.
- 17 Wu G, Cai Y, Detection of a semirough target in turbulent atmosphere by a partially coherent beam, *Opt. Lett.* **36**, 1939 (2011). <https://doi.org/10.1364/OL.36.001939>.
- 18 Lajunen H, Saastamoinen T, Propagation characteristics of partially coherent beams with spatially varying correlations, *Opt. Lett.* **36**, 4104 (2011). <https://doi.org/10.1364/OL.36.004104>.
- 19 Cai Y, Chen Y, Wang F, Generation and propagation of partially coherent beams with nonconventional correlation functions: a review, *J. Opt. Soc. Am. A* **31**, 2083 (2014). <https://doi.org/10.1364/JOSAA.31.002083>.
- 20 Rodenburg B, Mirhosseini M, Magaña-Loaiza OS, Boyd RW, Experimental generation of an optical field with arbitrary spatial coherence properties, *J. Opt. Soc. Am. B* **31**, A51 (2014). <https://doi.org/10.1364/JOSAB.31.000A51>.
- 21 Divitt S, Novotny L, Spatial coherence of sunlight and its implications for light management in photovoltaics, *Optica* **2**, 95 (2015). <https://doi.org/10.1364/OPTICA.2.000095>.
- 22 Chen Y, Ponomarenko SA, Cai Y, Experimental generation of optical coherence lattices, *Appl. Phys. Lett.* **109**, 061107 (2016). <https://doi.org/10.1063/1.4960966>.
- 23 M.W. Hyde IV MW, Bose-Pillai SR, Wood RA, Synthesis of non-uniformly correlated partially coherent sources using a deformable mirror, *Appl. Phys. Lett.* **111**, 101106 (2017). <https://doi.org/10.1063/1.4994669>.
- 24 Santarsiero M, Martínez-Herrero R, Maluenda D, de Sande JCG, Piquero G, Gori F, Partially coherent sources with circular coherence, *Opt. Lett.* **42**, 1512 (2017). <https://doi.org/10.1364/OL.42.001512>.
- 25 Santarsiero M, Martínez-Herrero R, Maluenda D, de Sande JCG, Piquero G, Gori F, Synthesis of circularly coherent sources, *Opt. Lett.* **42**, 4115 (2017). <https://doi.org/10.1364/OL.42.004115>.
- 26 Ding C, Koivurova M, Turunen J, Pan L, Self-focusing of a partially coherent beam with circular coherence, *J. Opt. Soc. Am. A* **34**, 1441 (2017). <https://doi.org/10.1364/JOSAA.34.001441>.
- 27 Piquero G, Santarsiero M, Martínez-Herrero R, de Sande JCG, Alonzo M, Gori F, Partially coherent sources with radial coherence, *Opt. Lett.* **43**, 2376 (2018). <https://doi.org/10.1364/OL.43.002376>.
- 28 Chen X, Li J, Rafsanjani SMH, Korotkova O, Synthesis of I_m -Bessel correlated beams via coherent modes, *Opt. Lett.* **43**, 3590 (2018). <https://doi.org/10.1364/OL.43.003590>.
- 29 Wu D, Wang F, Cai Y, High-order nonuniformly correlated beams, *Opt. Laser Technol.* **99**, 230 (2018). <https://doi.org/10.1016/j.optlastec.2017.09.007>.
- 30 Martínez-Herrero R, Piquero G, de Sande JCG, Santarsiero M, Gori F, Besinc pseudo-Schell model sources with circular coherence, *Appl. Sci. Basel* **9**, 2716 (2019). <https://doi.org/10.3390/app9132716>.
- 31 de Sande JCG, Martínez-Herrero R, Piquero G, Santarsiero M, Gori F, Pseudo-Schell model sources, *Opt. Express* **27**, 3963 (2019). <https://doi.org/10.1364/OE.27.003963>.
- 32 Zhu X, Yu J, Chen Y, Wang F, Korotkova O, Cai Y, Experimental synthesis of random light sources with circular coherence by digital micro-mirror device, *Appl. Phys. Lett.* **117**, 121102 (2020). <https://doi.org/10.1063/5.0024283>.
- 33 Martínez-Herrero R, Santarsiero M, Piquero G, de Sande JCG, A new type of shape-invariant beams with structured coherence: Laguerre-Christoffel-Darboux beams, *Photonics* **8**, 134 (2021). <https://doi.org/10.3390/photonics8040134>.
- 34 Santarsiero M, Martínez-Herrero R, Piquero G, de Sande JCG, Gori F, *Modal analysis of pseudo-Schell model sources*, *Photonics* **8**, 449 (2021). <https://doi.org/10.3390/photonics8100449>.
- 35 Martínez-Herrero R, Piquero G, Santarsiero M, Gori F, de Sande JCG, A class of vectorial pseudo-Schell model sources with structured coherence and polarization, *Opt. Laser Technol.* **152**, 108079 (2022). <https://doi.org/10.1016/j.optlastec.2022.108079>.
- 36 Korotkova O, Gbur G, in A Tribute to Emil Wolf. Progress in Optics, Vol. 65, edited by T.D. Visser (Elsevier, 2020), pp. 43–104.
- 37 Moreno-Acosta P, Rickenstorff-Parrao C, Ramirez-San-Juan JC, Rosales-Guzman C, Ramos-Garcia R, Experimental generation of partially coherent besinc pseudo-Schell model sources using a digital micromirror device, *J. Opt. Soc. Am. B* **42**, 1804 (2025). <https://doi.org/10.1364/JOSAB.564315>.
- 38 Gori F, Santarsiero M, Martínez-Herrero R, Uni-variable cross-spectral densities, *Opt. Laser Technol.* **180**, 111511 (2025). <https://doi.org/10.1016/j.optlastec.2024.111511>.
- 39 Indebetouw G, Optical vortices and their propagation, *J. Mod. Opt.* **40**, 73 (1993). <https://doi.org/10.1080/09500349314550101>.
- 40 Simon R, Mukunda N, Twisted Gaussian Schell-model beams, *J. Opt. Soc. Am. A* **10**, 95 (1993). <https://doi.org/10.1364/JOSAA.10.000095>.
- 41 Gori F, Santarsiero M, Borghi R, Vicalvi S, Partially coherent sources with helicoidal modes, *J. Mod. Opt.* **45**, 539 (1998). <https://doi.org/10.1080/09500349808231913>.
- 42 Ponomarenko SA, A class of partially coherent beams carrying optical vortices, *J. Opt. Soc. Am. A* **18**, 150 (2001). <https://doi.org/10.1364/JOSAA.18.000150>.
- 43 Gbur G, Visser TD, Coherence vortices in partially coherent beams, *Opt. Commun.* **222**, 117 (2003). [https://doi.org/10.1016/S0030-4018\(03\)01606-7](https://doi.org/10.1016/S0030-4018(03)01606-7).
- 44 Tamburini F, Anzolin G, Umbriaco G, Bianchini A, Barbieri C, Overcoming the Rayleigh criterion limit with optical vortices, *Phys. Rev. Lett.* **97**, 163903 (2006). <https://doi.org/10.1103/PhysRevLett.97.163903>.

- 45 Franke-Arnold S, Allen L, Padgett M, Advances in optical angular momentum, *Laser Photonics Rev.* **2**, 299 (2008). <https://doi.org/10.1002/lpor.200810007>.
- 46 Padgett M, Bowman R, Tweezers with a twist, *Nat. Photonics* **5**, 343 (2011). <https://doi.org/10.1038/nphoton.2011.81>.
- 47 Mirhosseini M, Magaña-Loaiza OS, Chen C, Rodenburg B, Malik M, Boyd RW, Rapid generation of light beams carrying orbital angular momentum, *Opt. Express* **21**, 30196 (2013). <https://doi.org/10.1364/OE.21.030196>.
- 48 Ambuj A, Vyas R, Singh S, Diffraction of orbital angular momentum carrying optical beams by a circular aperture, *Opt. Lett.* **39**, 5475 (2014). <https://doi.org/10.1364/OL.39.005475>.
- 49 Gbur G, *Singular Optics*, 1st edn. (CRC Press, 2016), ISBN 978-0521642224.
- 50 Zeng J, Lin R, Liu X, Zhao C, Cai Y, Review on partially coherent vortex beams, *Front. Optoelectron.* **12**, 229 (2019). <https://doi.org/10.1007/s12200-019-0901-x>.
- 51 Zhang Y, Cai Y, Gbur G, Control of orbital angular momentum with partially coherent vortex beams, *Opt. Lett.* **44**, 3617 (2019). <https://doi.org/10.1364/OL.44.003617>.
- 52 Liu X, Zeng J, Cai Y, Review on vortex beams with low spatial coherence, *Adv. Phys. X* **4**, 1626766 (2019). <https://doi.org/10.1080/23746149.2019.1626766>.
- 53 Zhang H, Lu X, Wang Z, Konijnenberg AP, Wang H, Zhao C, Cai Y, Generation and propagation of partially coherent power-exponent-phase vortex beam, *Front. Phys.* **9**, 781688 (2021). <https://doi.org/10.3389/fphy.2021.781688>.
- 54 Hyde IV MW, Korotkova O, Spencer MF, Partially coherent sources whose coherent modes are spatiotemporal optical vortex beams, *J. Opt.* **25**, 035606 (2023). <https://doi.org/10.1088/2040-8986/acba2d>.
- 55 Mandel L, Wolf E, *Optical Coherence and Quantum Optics* (Cambridge University Press, 1995), ISBN 9780521417112.
- 56 Siegman AE, *Lasers* (University Science Books, 1986), ISBN 0935702113.
- 57 Korotkova O, Gbur G, Unified matrix representation for spin and orbital angular momentum in partially coherent beams, *Phys. Rev. A* **103**, 023529 (2021). <https://doi.org/10.1103/PhysRevA.103.023529>.
- 58 Korotkova O, Pokharel S, OAM degree of coherence, *Opt. Lett.* **49**, 5103 (2024). <https://doi.org/10.1364/OL.528291>.
- 59 Korotkova O, Orbitalization ellipse of a light beam, *Opt. Lett.* **50**, 391 (2025). <https://doi.org/10.1364/OL.545613>.
- 60 Korotkova O, Orbitalization structure of random light beams, *J. Opt.* **27**, 065606 (2025). <https://doi.org/10.1088/2040-8986/addc7c>.
- 61 Born M, Wolf E, *Principles of Optics*, 7th (corrected) edn. (Cambridge University Press, 1999), ISBN 978-0521642224.
- 62 Gradshteiin IS, Ryzhik IM, *Table of Integrals, Series, and Products*, 4th edn. (Academic Press, 1965).
- 63 Abramowitz M, Stegun I, eds., *Handbook of mathematical functions* (Dover Publications Inc, 1972).
- 64 Prudnikov A, Brychkov Y, Marichev O, *Integrals and Series, Vol. 1: Elementary Functions* (Gordon and Breach Science Publisher, 1986).